POLITECNICO DI TORINO
Repository ISTITUZIONALE

Sensorless Self-Commissioning of Synchronous Reluctance Motors at Standstill

Original
Sensorless Self-Commissioning of Synchronous Reluctance Motors at Standstill / Hinkkanen, Marko; Pescetto, Paolo; Molsa, Eemeli; Saarakkala, Seppo E.; Pellegrino, GIAN - MARIO LUIGI; Bojoi, IUSTIN RADU. - (2016). (Intervento presentato al convegno XXIIth International Conference on Electrical Machines (ICEM'2016) tenutosi a Losanna (CH) nel September 4-7, 2016) [10.1109/ICELMACH.2016.7732673].

Availability:
This version is available at: 11583/2649203 since: 2017-05-29T15:44:43Z

Publisher:
IEEE, 345 E 47TH ST, NEW YORK, NY 10017 USA

Published
DOI:10.1109/ICELMACH.2016.7732673

Terms of use:

This article is made available under terms and conditions as specified in the corresponding bibliographic description in the repository

Publisher copyright

(Article begins on next page)

18 April 2024

Sensorless Self-Commissioning of Synchronous Reluctance Motors at Standstill

Marko Hinkkanen, *Senior Member, IEEE,* Paolo Pescetto, Eemeli Mölsä, Seppo E. Saarakkala, Gianmario Pellegrino, *Senior Member, IEEE,* and Radu Bojoi, *Senior Member, IEEE*

***Abstract*—This paper proposes a standstill method for identification of the magnetic model of synchronous reluctance motors (SyRMs). The saturation and cross-saturation effects are properly taken into account. The motor is fed by an inverter with a short sequence of bipolar voltage pulses that are first applied on the rotor d- and q-axes separately and then simultaneously on both the axes. The stator flux linkages are computed by integrating the induced voltages. Using the current and flux samples, the parameters of an algebraic magnetic model are estimated by means of linear least squares. The proposed method is robust against the stator resistance variations and inverter nonlinearities due to the high test voltages (of the order of the rated voltage). The fitted model matches very well with the reference saturation characteristics, measured using a constant-speed method, and enables extrapolation outside the sample range. The method was tested with a 2.2-kW SyRM, whose shaft was uncoupled from any mechanical load, which is the most demanding condition for this method. The proposed method can be used for automatic self-commissioning of sensorless SyRM drives at standstill.**

***Index Terms*—Flux maps, identification, linear least squares (LLS), saturation characteristics.**

I. Introduction

Synchronous reluctance motors (SyRMs) are simple to manufacture, mechanically robust, and comparatively cheap. If properly controlled using the maximum-torque-per-ampere (MTPA) principle, their efficiency is better (or their frame size is smaller) than that of the corresponding induction motor. In order to be able to replace general-purpose induction motor drives in simple applications (pumps, fans, conveyors, etc.), the SyRM drives should be sensorless. The MTPA principle and sensorless control require a magnetic model, where the cross-saturation must be properly taken into account. For general purpose applications, the magnetic model of any unknown SyRM should be automatically identified at standstill during the drive start-up, using its power converter and embedded controller. This is a common practice in the case of induction motor drives, where various standstill self-commissioning algorithms have been available for the last 20 or more years, cf. e.g., [1], [2].

An accurate way to identify the magnetic model of a SyRM is to rotate it at a constant speed in a test rig by another speed-controlled motor drive. The machine under test is current controlled, and the flux linkages are calculated by means of the stator voltage equation. Such a constant-speed identification method can be considered as a reference method [3], [4], requiring a suitable test rig and off-line data processing. Based on similar principles, a self-commissioning procedure in [5] uses accelerations and decelerations to emulate loading conditions.

Dealing with standstill testing conditions, several identification and self-commissioning methods for SyRMs and interior-permanent-magnet motors have been proposed recently [6]–[13]. The methods in [6], [7], [12] apply current or voltage steps to the machine under test and compute the stator flux by integrating the induced stator voltage. These methods are sensitive to the stator resistance estimate and to the accuracy of the voltage signals. In [11], the operating-point incremental inductances are explored using an AC current signal, superimposed to a DC bias emulating different operating points. The saturation curves are constructed from the estimated incremental inductances and the polarity of the DC bias is switched to achieve zero mean torque and no motion.

The method proposed in [13] is very simple and fast. It resembles the ones in [6], [7], [12], but uses bipolar voltage steps of much larger magnitude (up to the rated voltage), thus making the flux estimate practically insensitive to the stator resistance and offset errors. In [13], the linear least squares (LLS) method was used to fit a piecewise-defined mathematical model to the measured samples. The cross-saturation effect is taken into account by dividing the cross-axis into segments, each of which has its own saturation curve and a set of fitted parameters. Overall, the method in [13] works well with self-axis identification, but the cross-saturation model is impractical for its high number of parameters and its moderate accuracy.

In this paper, we propose a standstill identification method, which uses a similar excitation signal as the method in [13], with emphasis on improving the magnetic model. The algebraic magnetic model from [14] is adopted here, having a good trade-off between the number of parameters and accuracy. The LLS method is used for estimating the model parameters from the scattered current and flux data coming from the self-commissioning tests. The modelling approach was validated using the experimental data of five other SyRMs. Detailed experimental results are provided for a 2.2-kW SyRM drive to demonstrate the effectiveness of the proposed method. The saturation curves and MTPA trajectory obtained with the proposed self-commissioning method are compared with the reference data from constant-speed identification.

This work was supported in part by ABB Oy and in part by the Academy of Finland.

M. Hinkkanen, E. Mölsä, and S. E. Saarakkala are with the Department of Electrical Engineering and Automation, Aalto University, Espoo, Finland (e-mail: marko.hinkkanen@aalto.fi; olli.molsa@aalto.fi; seppo.saarakkala@aalto.fi).

P. Pescetto, G. Pellegrino, and R. Bojoi are with the Department of Energy, Politecnico di Torino, Turin, Italy (e-mail: paolo.pescetto@polito.it; gianmario.pellegrino@polito.it; radu.bojoi@polito.it).

TABLE I
BEST FIT INTEGER EXPONENTS OF (5) FOR SIX SYRMS

Motor	Power (kW)	Speed (r/min)	S	T	U	V
CMP	0.9	3 600	6	1	1	0
EA3	2.2	1 500	5	1	1	0
EA4	4.0	1 500	5	1	1	0
ABB	6.7	1 500	6	1	1	0
PMP	7.5	1 500	8	1	3	0
Sicme	250	1 000	5	1	1	0

II. MOTOR MODEL

A. Fundamental Equations

The SyRM model in rotor coordinates is considered. The stator voltage equations are

$$\frac{\mathrm{d}\psi_\mathrm{d}}{\mathrm{d}t} = u_\mathrm{d} - R_\mathrm{s} i_\mathrm{d} + \omega_\mathrm{m}\psi_\mathrm{q} \tag{1a}$$

$$\frac{\mathrm{d}\psi_\mathrm{q}}{\mathrm{d}t} = u_\mathrm{q} - R_\mathrm{s} i_\mathrm{q} - \omega_\mathrm{m}\psi_\mathrm{d} \tag{1b}$$

where ψ_d and ψ_q are the flux-linkage components, u_d and u_q are the voltage components, ω_m is the electrical angular speed of the rotor, and R_s is the stator resistance. The current components

$$i_\mathrm{d} = i_\mathrm{d}(\psi_\mathrm{d}, \psi_\mathrm{q}) \qquad i_\mathrm{q} = i_\mathrm{q}(\psi_\mathrm{d}, \psi_\mathrm{q}) \tag{2}$$

are generally nonlinear functions of the flux components. They are the inverse of the flux maps extensively used in the literature [4]–[7], [11]–[13], often represented by two-dimensional look-up tables. Here, the modelling approach (2) is chosen, because it is more favourable towards representation in the algebraic form. Since the nonlinear inductor should not generate or dissipate electrical energy, the reciprocity condition [15]

$$\frac{\partial i_\mathrm{d}(\psi_\mathrm{d}, \psi_\mathrm{q})}{\partial \psi_\mathrm{q}} = \frac{\partial i_\mathrm{q}(\psi_\mathrm{d}, \psi_\mathrm{q})}{\partial \psi_\mathrm{d}} \tag{3}$$

should hold. Typically, the core losses are either omitted or modelled separately using a core-loss resistor in the model. The produced torque is

$$T_\mathrm{e} = \frac{3p}{2}\left(\psi_\mathrm{d} i_\mathrm{q} - \psi_\mathrm{q} i_\mathrm{d}\right) \tag{4}$$

where p is the number of pole pairs. If the functions (2) and the stator resistance are known, the machine is fully characterized both in the steady and transient states. For example, the MTPA trajectory can be resolved from (2) and (4).

B. Algebraic Magnetic Model

In this paper, the saturation characteristics (2) are modelled by the algebraic functions [14]

$$i_\mathrm{d} = \psi_\mathrm{d}\left(a_\mathrm{d0} + a_\mathrm{dd}|\psi_\mathrm{d}|^S + \frac{a_\mathrm{dq}}{V+2}|\psi_\mathrm{d}|^U|\psi_\mathrm{q}|^{V+2}\right) \tag{5a}$$

$$i_\mathrm{q} = \psi_\mathrm{q}\left(a_\mathrm{q0} + a_\mathrm{qq}|\psi_\mathrm{q}|^T + \frac{a_\mathrm{dq}}{U+2}|\psi_\mathrm{d}|^{U+2}|\psi_\mathrm{q}|^V\right) \tag{5b}$$

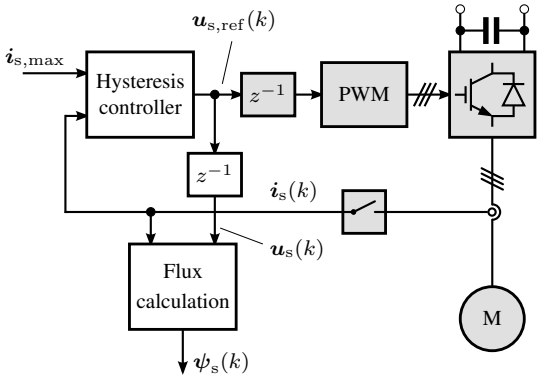

Fig. 1. Sensorless identification setup. The white blocks represent the control algorithm. The grey blocks model the plant: motor, converter, PWM, sampling, and computational time delay z^{-1}. The vector representation is used: $\boldsymbol{i}_\mathrm{s} = [i_\mathrm{d}, i_\mathrm{q}]^\mathrm{T}$, $\boldsymbol{u}_\mathrm{s} = [u_\mathrm{d}, u_\mathrm{q}]^\mathrm{T}$ and similarly for other vectors.

where a_d0, a_dd, a_q0, a_qq, and a_dq are nonnegative coefficients and S, T, U, and V are nonnegative exponents.[1] There are three parameters for the d-axis, three for the q-axis, and three for the cross-saturation. It can be seen that the reciprocity condition (3) holds. The use of the algebraic model instead of look-up tables makes the self-commissioning problem easier. The number of parameters to be identified is reduced. The parameters are extracted by fitting the model to the data from a reduced number of tests, which reduces the duration of the commissioning and simplifies data processing.

The algebraic model (5) was further simplified by using only selected integers as exponents. In order to study the typical range of the exponents, the model was fitted to the saturation data of six different SyRMs, measured using the constant-speed method. The best fit exponents are given in Table I. It can be noticed that $T = 1$ and $V = 0$ hold for all the motors and $U = 1$ holds for five motors out of six. Optimal values of S vary between 5 and 8. Furthermore, a choice of S is not critical: the deviation of ± 1 from the optimal value still gives good accuracy.

III. IDENTIFICATION METHOD

A. Test Sequences

The test procedure proposed in [13] is briefly reviewed and illustrated with measured waveforms of a 2.2-kW SyRM drive. The rated line-line rms voltage of the motor is 400 V and the rated rms current is 5.1 A. Fig. 1 shows the sensorless controller used in the tests. The control scheme has been implemented on a dSPACE DS1103 board. The sampling of the currents is synchronized with the PWM operation. The sampling and switching period is $T_\mathrm{s} = 100$ μs. In all the tests, the shaft of the motor was free (without any additional inertia connected to it) and no motion sensor was used. This condition is considered as the worst case for sensorless identification at standstill, since it is challenging to avoid that the current excitation makes the rotor move.

[1] If needed, (5) could also be expressed as inductance functions: $L_\mathrm{d}(\psi_\mathrm{d}, \psi_\mathrm{q}) = \psi_\mathrm{d}/[i_\mathrm{d}(\psi_\mathrm{d}, \psi_\mathrm{q})]$ and $L_\mathrm{q}(\psi_\mathrm{d}, \psi_\mathrm{q}) = \psi_\mathrm{q}/[i_\mathrm{q}(\psi_\mathrm{d}, \psi_\mathrm{q})]$.

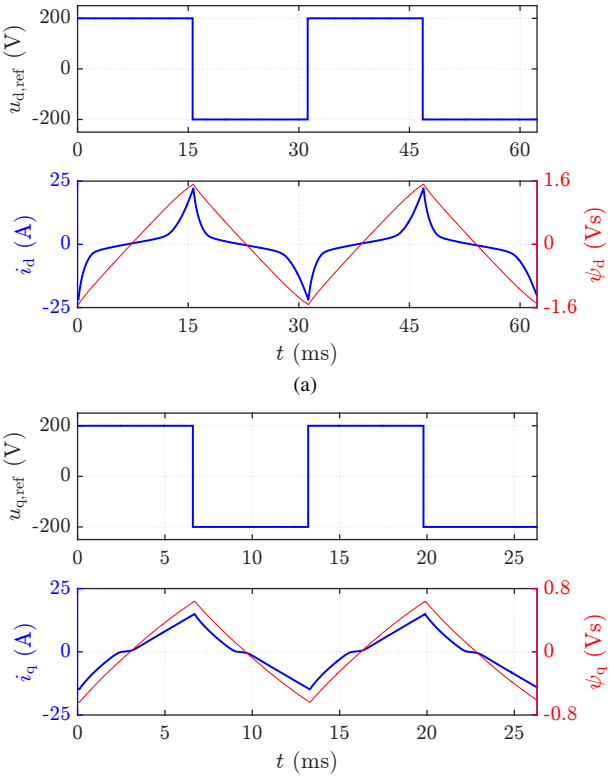

Fig. 2. Measured self-axis test waveforms: (a) d-axis; (b) q-axis. The upper subplots show the voltages. The lower subplots show the measured currents and the calculated fluxes. The parameters are $u_{\mathrm{d,out}} = u_{\mathrm{q,out}} = 200$ V, $i_{\mathrm{d,max}} = 20$ A, and $i_{\mathrm{q,max}} = 14$ A. The number of samples is $N_{\mathrm{d}} = 624$ in the d-axis test and $N_{\mathrm{q}} = 264$ in the q-axis test.

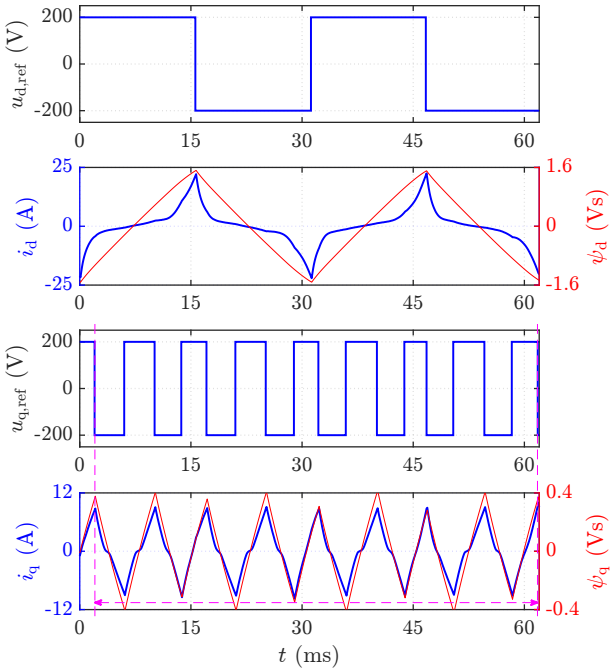

Fig. 3. Measured waveforms of the cross-saturation test, where both the axes are simultaneously excited. The first two subplots show the data for the d-axis and the last two subplots show the data for the q-axis. The parameters are $u_{\mathrm{d,out}} = u_{\mathrm{q,out}} = 200$ V, $i_{\mathrm{d,max}} = 20$ A, and $i_{\mathrm{q,max}} = 8$ A. The number of samples is $N_{\mathrm{dq}} = 621$. The average value of the q-axis flux was calculated from the complete cycles (the interval $t = 2.0 \ldots 61.8$ ms marked in the figure).

Only the initial position of the d-axis should be known, since it is assumed that the rotor does not considerably move during the test. If moving the rotor is possible, the DC-current vector can be fed to the desired direction (e.g. the a-phase magnetic axis) before the test, which causes the rotor to rotate into this direction. Alternatively, the initial rotor position can be found using a signal-injection method, without causing the rotor movement. The results shown in the following were measured after parking the rotor using the DC current. The signal-injection method was also tested, as commented in the following.

1) d-Axis Test: A simple hysteresis controller is used. In the d-axis test, the control law is

$$u_{\mathrm{d,ref}}(k) = \begin{cases} u_{\mathrm{d,out}} & \text{if } i_{\mathrm{d}}(k) < -i_{\mathrm{d,max}} \\ -u_{\mathrm{d,out}} & \text{if } i_{\mathrm{d}}(k) > i_{\mathrm{d,max}} \\ u_{\mathrm{d,ref}}(k-1) & \text{otherwise} \end{cases} \tag{6a}$$

$$u_{\mathrm{q,ref}}(k) = 0 \tag{6b}$$

where $u_{\mathrm{d,out}}$ is the test-voltage magnitude, $i_{\mathrm{d,max}}$ is the current limit, and k is the discrete-time index. The current limit defines the current span, i.e. the range of identification. It can be selected to be, e.g., twice the rated current. In the d-axis test, the torque is ideally zero and the operating point is stable even at free shaft.

Fig. 2(a) shows the measured waveforms of the d-axis test. The voltage $u_{\mathrm{d}}(k) = u_{\mathrm{d,ref}}(k-1)$ is used in the flux calculation. The samples of two complete cycles, shown in the figure, are used in the identification. The zero-crossings are detected from the reference voltage $u_{\mathrm{d,ref}}(k)$. The data of one complete cycle would suffice for identification, but two cycles are used here for better illustration. The test voltage is $u_{\mathrm{d,out}} = 200$ V and the current limit is $i_{\mathrm{d,max}} = 20$ A (which is almost three times the rated current).

2) q-Axis Test: The control law in the q-axis test is analogous to (6). The torque is ideally zero also in the q-axis test, but the operating point is only marginally stable. If the rotor is free to rotate, the current limit $i_{\mathrm{q,max}}$ should be selected low enough to avoid the rotor movement. Fig. 2(b) shows the measured waveforms of the q-axis test. As in the case of the d-axis test, the samples of two complete cycles are shown and used in the identification. The test voltage is $u_{\mathrm{q,out}} = 200$ V and the current limit is $i_{\mathrm{q,max}} = 14$ A. As the rotor was positioned with the DC current before the test, this test condition could be used for several seconds without the rotor movement. Instead, when the initial rotor position was estimated using signal injection and $i_{\mathrm{q,max}} = 14$ A was used, the rotor moved less than five electrical degrees during the first two complete cycles, due to inaccuracies in the initial position estimate and the voltage production. The rotor movement can be decreased or avoided by decreasing the limit $i_{\mathrm{q,max}}$. Alternatively, if the rotor moves during the q-axis test, it means that the rotor can be parked into a more

stable initial position, and the test can be repeated using the full current range (14 A in this case).

3) Cross-Saturation Test: The hysteresis controllers corresponding to (6a) are simultaneously used in the d- and q-axes. The torque varies during the test, but the average torque is approximately zero. Fig. 3 shows the measured waveforms of the cross-saturation test. The samples of two complete d-axis cycles are used in the identification. The test voltages are 200 V and the current limits are $i_{\mathrm{d,max}} = 20$ A and $i_{\mathrm{q,max}} = 8$ A. During the sequence shown in Fig. 3, the rotor angle varied less than 10 electrical degrees. When the initial rotor position was detected using signal injection, the same current limits could be used.

B. Flux Calculation

The flux linkages are calculated using the forward Euler approximation

$$\psi_{\mathrm{d}}(k+1) = \psi_{\mathrm{d}}(k) + T_{\mathrm{s}}[u_{\mathrm{d}}(k) - R_{\mathrm{s}} i_{\mathrm{d}}(k)] \tag{7}$$

The analogous equation is used for the q-axis. The estimate for the stator resistance is obtained simply by feeding the DC current into the stator before the test sequences. Inverter nonlinearities could be identified and compensated for, but they are omitted in this paper because the proposed method works fine also without the compensation.

In the self-axis tests, the samples consist of complete cycles. The average of the flux samples is calculated and removed from the samples. Fig. 2 shows the waveforms of the calculated flux samples after the average value is removed. Using the same data, the currents are plotted as functions of the fluxes in Fig. 4(a). It can be seen that the two cycles almost perfectly overlap. The dashed lines in the figure show the reference saturation curves, which have been measured using the constant-speed method [4]. If $R_{\mathrm{s}} = 0$ is used in (7), the hysteresis loops become slightly thicker, but their shape remains similar, as demonstrated in Fig. 4(b). In the results of this paper, the measured stator resistance value $R_{\mathrm{s}} = 3.6$ Ω is used, but assuming $R_{\mathrm{s}} = 0$ would lead to similar results.

In the cross-saturation test, the d-axis samples have complete cycles, but the q-axis samples generally include an incomplete cycle (in addition to several complete cycles), which may distort the average. Hence, to minimize this distortion, the average value of the q-axis flux is calculated using only the complete cycles (cf. the interval marked with the vertical dashed lines in Fig. 3) and removed from all the samples.

C. LLS Method

If the exponents of the magnetic model (5) are fixed, the remaining five parameters can be conveniently estimated using the LLS method. The estimation problem reduces to solving a set of linear equations: there is a unique solution and neither initial values nor cost functions are needed. A recursive variant of the LLS method can be implemented in embedded processors used in converters. Since the amount of

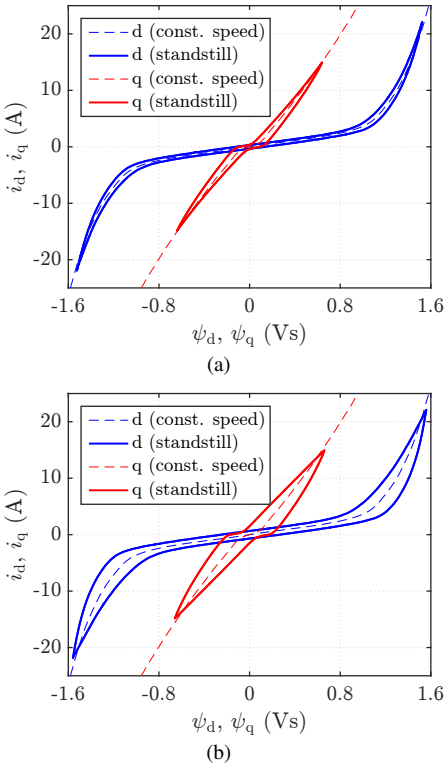

Fig. 4. Measured self-axis saturation characteristics: (a) $R_{\mathrm{s}} = 3.6$ Ω is used; (b) $R_{\mathrm{s}} = 0$ is assumed. In neither cases are the inverter nonlinearities compensated for. The blue curves show the current i_{d} at $i_{\mathrm{q}} = 0$ as a function of ψ_{d}. The red curves show i_{q} at $i_{\mathrm{d}} = 0$ as a function of ψ_{q}. In (a), the solid lines are drawn using the data from Fig. 2. The dashed lines show the reference saturation curves, measured using the constant-speed method.

feasible integer exponents is limited as discussed in Section II-B, the parameters can be solved for different sets of exponents, which have been chosen in advance. Then, the set of exponents (and the corresponding fitted parameters) leading to the smallest sum of the squared residuals can be chosen. The data collected during the three tests (d-axis, q-axis, and cross-saturation tests) are used in three consecutive fits, as explained below.

1) d-Axis Fit: Assuming positive current and flux samples, the model (5) for the d-axis reduces to

$$i_{\mathrm{d}} = a_{\mathrm{d0}} \psi_{\mathrm{d}} + a_{\mathrm{dd}} \psi_{\mathrm{d}}^{S+1} \tag{8}$$

when only the d-axis is excited. If the exponent S is fixed, this model is linear with respect to the unknown parameters a_{d0} and a_{dd}. The LLS problem in a vector form is

$$\underbrace{\begin{bmatrix} i_{\mathrm{d}}(1) \\ i_{\mathrm{d}}(2) \\ \vdots \\ i_{\mathrm{d}}(N_{\mathrm{d}}) \end{bmatrix}}_{\boldsymbol{y}_{\mathrm{d}}} = \underbrace{\begin{bmatrix} \psi_{\mathrm{d}}(1) & \psi_{\mathrm{d}}(1)^{S+1} \\ \psi_{\mathrm{d}}(2) & \psi_{\mathrm{d}}(2)^{S+1} \\ \vdots & \vdots \\ \psi_{\mathrm{d}}(N_{\mathrm{d}}) & \psi_{\mathrm{d}}(N_{\mathrm{d}})^{S+1} \end{bmatrix}}_{\boldsymbol{X}_{\mathrm{d}}} \underbrace{\begin{bmatrix} a_{\mathrm{d0}} \\ a_{\mathrm{dd}} \end{bmatrix}}_{\boldsymbol{\beta}_{\mathrm{d}}} + \underbrace{\begin{bmatrix} \varepsilon_{\mathrm{d}}(1) \\ \varepsilon_{\mathrm{d}}(2) \\ \vdots \\ \varepsilon_{\mathrm{d}}(N_{\mathrm{d}}) \end{bmatrix}}_{\boldsymbol{\varepsilon}_{\mathrm{d}}} \tag{9}$$

where $\boldsymbol{y}_{\mathrm{d}}$ is the vector of the current samples, $\boldsymbol{X}_{\mathrm{d}}$ is regressor matrix, $\boldsymbol{\beta}_{\mathrm{d}}$ is the parameter vector, $\boldsymbol{\varepsilon}_{\mathrm{d}}$ is the residual vector,

TABLE II
FITTED PARAMETERS GIVEN IN SI UNITS

S	T	U	V	a_{d0}	a_{dd}	a_{q0}	a_{qq}	a_{dq}
5	1	1	0	2.41	1.47	12.8	17.0	13.2

and N_{d} is the number of samples. The sum of the squared residuals is

$$J_{\mathrm{d}}(\boldsymbol{\beta}_{\mathrm{d}}) = \boldsymbol{\varepsilon}_{\mathrm{d}}^{\mathrm{T}}\boldsymbol{\varepsilon}_{\mathrm{d}} \tag{10}$$

The parameter vector minimizing J_{d} is

$$\boldsymbol{\beta}_{\mathrm{d}} = (\boldsymbol{X}_{\mathrm{d}}^{\mathrm{T}}\boldsymbol{X}_{\mathrm{d}})^{-1}\boldsymbol{X}_{\mathrm{d}}^{\mathrm{T}}\boldsymbol{y}_{\mathrm{d}} \tag{11}$$

The fitting can be carried out using pre-selected values for the exponent S, and the best value can be chosen based on (10).

2) q-Axis Fit: The parameters estimation procedure for the q-axis is fully analogous to the that of the d-axis. The parameter vector is $\boldsymbol{\beta}_{\mathrm{q}} = [a_{\mathrm{q0}}, a_{\mathrm{qq}}]^{\mathrm{T}}$ and the number of samples is N_{q}.

3) Cross-Saturation Fit: The model (5) can be rewritten as

$$i_{\mathrm{d}} - a_{\mathrm{d0}}\psi_{\mathrm{d}} - a_{\mathrm{dd}}\psi_{\mathrm{d}}^{S+1} = \frac{a_{\mathrm{dq}}}{V+2}\psi_{\mathrm{d}}^{U+1}\psi_{\mathrm{q}}^{V+2} \tag{12a}$$

$$i_{\mathrm{q}} - a_{\mathrm{q0}}\psi_{\mathrm{q}} - a_{\mathrm{qq}}\psi_{\mathrm{q}}^{T+1} = \frac{a_{\mathrm{dq}}}{U+2}\psi_{\mathrm{d}}^{U+2}\psi_{\mathrm{q}}^{V+1} \tag{12b}$$

Since the parameters a_{d0}, a_{dd}, a_{q0}, and a_{qq} are known, the output vector

$$\boldsymbol{y}_{\mathrm{dq}} = \begin{bmatrix} i_{\mathrm{d}}(1) - a_{\mathrm{d0}}\psi_{\mathrm{d}}(1) - a_{\mathrm{dd}}\psi_{\mathrm{d}}(1)^{S+1} \\ i_{\mathrm{q}}(1) - a_{\mathrm{q0}}\psi_{\mathrm{q}}(1) - a_{\mathrm{qq}}\psi_{\mathrm{q}}(1)^{T+1} \\ \vdots \\ i_{\mathrm{d}}(N_{\mathrm{dq}}) - a_{\mathrm{d0}}\psi_{\mathrm{d}}(N_{\mathrm{dq}}) - a_{\mathrm{dd}}\psi_{\mathrm{d}}(N_{\mathrm{dq}})^{S+1} \\ i_{\mathrm{q}}(N_{\mathrm{dq}}) - a_{\mathrm{q0}}\psi_{\mathrm{q}}(N_{\mathrm{dq}}) - a_{\mathrm{qq}}\psi_{\mathrm{q}}(N_{\mathrm{dq}})^{T+1} \end{bmatrix} \tag{13}$$

is chosen, where N_{dq} is the number of samples. The regressor matrix is

$$\boldsymbol{X}_{\mathrm{dq}} = \begin{bmatrix} \frac{1}{V+2}\psi_{\mathrm{d}}(1)^{U+1}\psi_{\mathrm{q}}(1)^{V+2} \\ \frac{1}{U+2}\psi_{\mathrm{d}}(1)^{U+2}\psi_{\mathrm{q}}(1)^{V+1} \\ \vdots \\ \frac{1}{V+2}\psi_{\mathrm{d}}(N_{\mathrm{dq}})^{U+1}\psi_{\mathrm{q}}(N_{\mathrm{dq}})^{V+2} \\ \frac{1}{U+2}\psi_{\mathrm{d}}(N_{\mathrm{dq}})^{U+2}\psi_{\mathrm{q}}(N_{\mathrm{dq}})^{V+1} \end{bmatrix} \tag{14}$$

The cross-saturation parameter is estimated as

$$a_{\mathrm{dq}} = (\boldsymbol{X}_{\mathrm{dq}}^{\mathrm{T}}\boldsymbol{X}_{\mathrm{dq}})^{-1}\boldsymbol{X}_{\mathrm{dq}}^{\mathrm{T}}\boldsymbol{y}_{\mathrm{dq}} \tag{15}$$

IV. RESULTS

A. Fitting

Using the proposed method, the magnetic model (5) is fitted to the measured current and flux samples, shown in Figs. 2 and 3 in the time domain. The fitted parameters are given in Table II. Fig. 5 shows the mesh surfaces, which are plotted using the fitted parameters in the model (5). Also the samples are plotted in Fig. 5.

Fig. 6 compares the fitted model with the reference data from the constant-speed method [4]. It can be seen that the fitted model matches very well with real saturation characteristics also in the cross-saturation region.

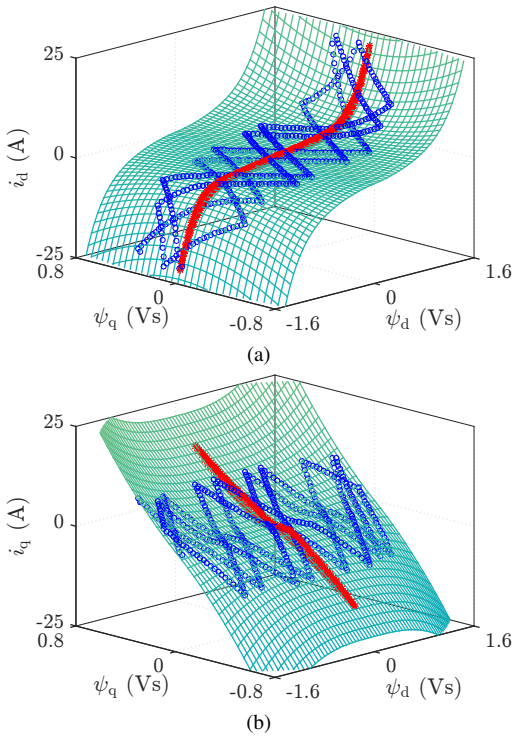

Fig. 5. Currents as functions of fluxes: (a) i_{d}; (b) i_{q}. The mesh surfaces correspond to the fitted model (5). The red stars show the measured samples from the self-axis saturation tests, cf. Fig. 2. The blue circles show the measured samples from the cross-saturation test, cf. Fig. 3.

As a comparison, the method [13] would need tens of parameters to model the cross-saturation and separate post-processing and interpolation algorithms should be implemented. On the contrary, only one parameter, a_{dq}, is needed in the proposed method to model the effect of the cross-saturation (since the exponents $U = 1$ and $V = 0$ can be typically used). The application of the proposed model and identification method is also more straightforward.

B. MTPA as an Application Example

Fig. 7(a) shows three MTPA trajectories for the motor under test. The stars represent the reference MTPA trajectory, measured using the constant-speed method. The red line shows the MTPA trajectory calculated using the magnetic model (5) and the fitted parameters in Table II. The blue dashed line represents the trajectory, which is also calculated using the model (5), but the cross-saturation is omitted by setting $a_{\mathrm{dq}} = 0$. It can be seen that the proposed method gives a trajectory, which is very close to the reference one. Fig. 7(b) compares the torque factors related to these three trajectories. The torque factor corresponding to the proposed method agrees very well with the the reference trajectory, also in overload conditions.

It is also worth noticing that the magnetic model (5) has been used in sensorless control, e.g., in [14], [16]. Hence, the

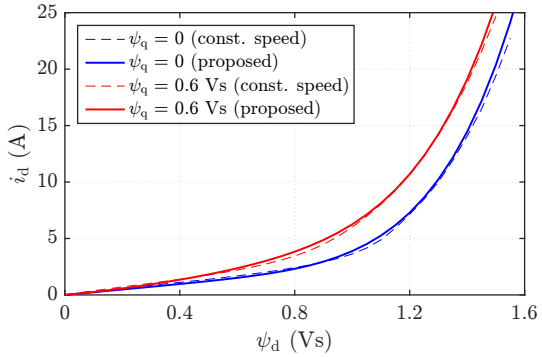

(a)

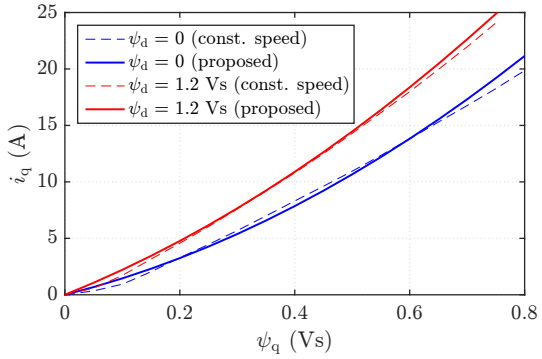

(b)

Fig. 6. Currents as functions of the fluxes: (a) i_d as a function of ψ_d for $\psi_\mathrm{q} = 0$ and $\psi_\mathrm{q} = 0.6$ Vs; (b) i_q as a function of ψ_q for $\psi_\mathrm{d} = 0$ and $\psi_\mathrm{d} = 1.2$ Vs. The dashed lines show the reference data, which has been measured using constant-speed identification. The solid lines show the results from the proposed standstill method.

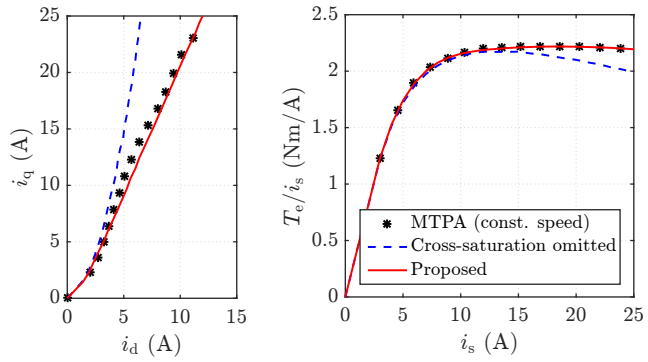

(a) (b)

Fig. 7. Comparison of MTPA characteristics: (a) control trajectories; (b) torque factors. The legends given in (b) hold for (a) as well. The current magnitude is denoted by i_s. The stars show the reference data from the constant-speed method. The red solid curves are calculated using the model (5) and the fitted parameters. In the case of the blue dashed curves, the cross-saturation is omitted by setting $a_\mathrm{dq} = 0$.

proposed self-commissioning method can be directly used in connection with these methods.

V. Conclusion

The identification method proposed in this paper combines the test sequence of [13], the algebraic magnetic model of [14], and the LLS method to determine the saturation characteristics of SyRMs at standstill. The cross-saturation effect is included. The method is robust against errors in the stator resistance and inverter voltage, due to the high test voltages. The algebraic magnetic model is physically feasible, it has few parameters, it takes the cross-saturation inherently into account, and it enables extrapolation outside the measured data range. The accuracy of the method has been compared with the reference data from constant-speed identification. The fitted model matches very well with real saturation characteristics also in the cross-saturation region. The proposed method can be used for automatic self-commissioning of sensorless SyRM drives.

References

[1] M. Ruff and H. Grotstollen, "Off-line identification of the electrical parameters of an industrial servo drive system," in *Conf. Rec. IEEE-IAS Annu. Meeting*, vol. 1, San Diego, CA, Oct. 1996, pp. 213–220.

[2] L. Peretti and M. Zigliotto, "Automatic procedure for induction motor parameter estimation at standstill," *IET Electr. Power Appl.*, vol. 6, no. 4, pp. 214–224, Apr. 2012.

[3] K. M. Rahman and S. Hiti, "Identification of machine parameters of a synchronous motor," *IEEE Trans. Ind. Appl.*, vol. 41, no. 2, pp. 557–565, Mar./Apr. 2005.

[4] E. Armando, R. Bojoi, P. Guglielmi, G. Pellegrino, and M. Pastorelli, "Experimental identification of the magnetic model of synchronous machines," *IEEE Trans. Ind. Appl.*, vol. 49, no. 5, pp. 2116–2125, Sept. 2013.

[5] G. Pellegrino, B. Boazzo, and T. Jahns, "Magnetic model self-identification for PM synchronous machine drives," *IEEE Trans. Ind. Appl.*, vol. 51, no. 3, pp. 2246–2254, May 2015.

[6] B. Štumberger, G. Štumberger, D. Dolinar, A. Hamler, and M. Trlep, "Evaluation of saturation and cross-magnetization effects in interior permanent-magnet synchronous motor," *IEEE Trans. Ind. Appl.*, vol. 39, no. 5, pp. 1264–1271, Sept./Oct. 2003.

[7] G. Štumberger, T. Marčič, B. Štumberger, and D. Dolinar, "Experimental method for determining magnetically nonlinear characteristics of electric machines with magnetically nonlinear and anisotropic iron core, damping windings, and permanent magnets," *IEEE Trans. Magn.*, vol. 44, no. 11, pp. 4341–4344, Nov. 2008.

[8] D. Uzel and Z. Peroutka, "Optimal control and identification of model parameters of traction interior permanent magnet synchronous motor drive," in *Proc. IEEE IECON 2011*, Melbourne, Australia, Nov. 2011, pp. 1960–1965.

[9] S. Ebersberger and B. Piepenbreier, "Identification of differential inductances of permanent magnet synchronous machines using test current signal injection," in *Proc. SPEEDAM 2012*, Sorrento, Italy, June 2012, pp. 1342–1347.

[10] I. Omrane, E. Etien, O. Bachelier, and W. Dib, "A simplified least squares identification of permanent magnet synchronous motor parameters at standstill," in *Proc. IEEE IECON 2013*, Vienna, Austria, Nov. 2013, pp. 2578–2583.

[11] S. Odhano, R. Bojoi, S. Rosu, and A. Tenconi, "Identification of the magnetic model of permanent-magnet synchronous machines using DC-biased low-frequency AC signal injection," *IEEE Trans. Ind. Appl.*, vol. 51, no. 4, pp. 3208–3215, July 2015.

[12] L. Peretti, P. Sandulescu, and G. Zanuso, "Self-commissioning of flux linkage curves of synchronous reluctance machines in quasi-standstill condition," *IET Electr. Power Appl.*, vol. 9, no. 9, pp. 642–651, 2015.

[13] N. Bedetti, S. Calligaro, and R. Petrella, "Stand-still self identification of flux characteristics for SynRM using novel saturation approximating function and multiple linear regression," in *Proc. IEEE ECCE 2015*, Montreal, Canada, Sept. 2015, pp. 2995–3002.

[14] Z. Qu, T. Tuovinen, and M. Hinkkanen, "Inclusion of magnetic saturation in dynamic models of synchronous reluctance motors," in *Proc. ICEM'12*, Marseille, France, Sept. 2012, pp. 994–1000.

[15] A. Vagati, M. Pastorelli, F. Scapino, and G. Franceschini, "Impact of cross saturation in synchronous reluctance motors of the transverse-laminated type," *IEEE Trans. Ind. Appl.*, vol. 36, no. 4, pp. 1039–1046, Jul./Aug. 2000.

[16] T. Tuovinen and M. Hinkkanen, "Adaptive full-order observer with high-frequency signal injection for synchronous reluctance motor drives," *IEEE J. Emerg. Sel. Topics Power Electron.*, vol. 2, no. 2, pp. 181–189, June 2014.

Marko Hinkkanen (M'06–SM'13) received the M.Sc.(Eng.) and D.Sc.(Tech.) degrees from Helsinki University of Technology, Espoo, Finland, in 2000 and 2004, respectively. He is currently an Assistant Professor with the School of Electrical Engineering, Aalto University, Espoo. He has authored or co-authored more than 100 technical papers of which over 30 in IEEE journals. His research interests include control systems, electric drives, and power converters. Dr. Hinkkanen is an Editorial Board Member of the IET ELECTRIC POWER APPLICATIONS.

Paolo Pescetto is a PhD student at the Politecnico di Torino, Turin, Italy. He received the Bachelor and Master degrees from the same university in 2013 and 2015, respectively, with full grade and honours in both cases. His current research interests include synchronous motor drives, sensorless control and self-commissioning techniques. Mr. Pescetto has one conference paper, published in 2015 in cooperation with the Norwegian University of Science and Technology, where he was an Erasmus+ student. The paper received the Best Paper Award in Renewable Energies at the EVER15 conference.

Eemeli Mölsä received the B.Eng. degree in electrical engineering from Metropolia University of Applied Sciences, Helsinki, Finland in 2012 and M.Sc.(Tech.) degree in electrical engineering from Aalto University, Espoo, Finland in 2015. He is currently working toward the D.Sc.(Tech.) degree at Aalto University. His main research interest is the control of electrical drives.

Seppo E. Saarakkala received the M.Sc.(Eng.) degree from Lappeenranta University of Technology, Lappeenranta, Finland, in 2008 and the D.Sc.(Tech.) degree from Aalto University, Espoo, Finland, in 2014. Since 2010, he has been with the School of Electrical Engineering, Aalto University, Espoo, Finland, where he is currently a Post-Doctoral Research Scientist.

Gianmario Pellegrino (M'06–SM'13), PhD, is an Associate Professor of Electrical Machines and Drives at the Politecnico di Torino, Turin, Italy. Dr. Pellegrino is engaged in several research projects with the industry, and has 30 journal papers, one patent and four Best Paper Awards received from IEEE. He was a visiting fellow at Aalborg University, Denmark, in 2002, at the University of Nottingham, UK, in 2010, and at the University of Wisconsin-Madison, USA, in 2013. Dr. Pellegrino is an Associate Editor for the IEEE TRANSACTIONS ON INDUSTRY APPLICATIONS.

Radu Bojoi (SM'10) received the M.Sc. degree in electrical engineering from the Gheorghe Asachi Technical University, Iasi, Romania, in 1993 and the Ph.D. degree from the Politecnico di Torino, Turin, Italy, in 2003. From 1994 to 1999, he was an Assistant Professor with the Department of Electrical Drives and Industrial Automation, Gheorghe Asachi Technical University. In 2004, he joined the Department of Energy, Politecnico di Torino, where he is currently an Associate Professor of electrical drives and power electronics. He has published more than 100 papers in international conference proceedings and technical journals. His scientific interests include the design and development of digital control systems in the fields of power electronics, electrical drives, and power-conditioning systems. Dr. Bojoi is an Associate Editor of the IEEE TRANSACTIONS ON INDUSTRY APPLICATIONS and the IEEE TRANSACTIONS ON INDUSTRIAL ELECTRONICS.